Hindawi
Journal of Sensors
Volume 2022, Article ID 8980198, 10 pages
https://doi.org/10.1155/2022/8980198

Research Article

Research on Working Memory States Based on Weighted K-Order Propagation Number Algorithm: An EEG Perspective

Yao Chen,[1] Yuhong Zhang,[2] Weiwei Ding,[1] Fachang Cui,[1] and Liya Huang[1,3]

[1]*College of Electronic and Optical Engineering & College of Flexible Electronics, Nanjing University of Posts and Telecommunications, Nanjing, China*
[2]*College of Automation and College of Artificial Intelligence, Nanjing University of Posts and Telecommunications, Nanjing, China*
[3]*National and Local Joint Engineering Laboratory of RF Integration and Micro-Assembly Technology, Nanjing, China*

Correspondence should be addressed to Liya Huang; huangly@njupt.edu.cn

Received 27 April 2022; Accepted 26 June 2022; Published 11 July 2022

Academic Editor: Rocio Perez de Prado

Working memory (WM) is considered the mental workplace that retains and manipulates information. This study investigates the internal mechanism in WM states from an electroencephalography (EEG) network perspective. Firstly, we devised a novel letter-sequence version of the n-back experiment to collect EEG data, analyzed the neural oscillations in the theta and gamma bands, and then constructed Phase Lock Value (PLV) grounded brain networks to examine the synchronizations among dissimilar brain regions. The complex topology properties (e.g., global efficiency, local efficiency, and small-worldness) were scrutinized as well. Additionally, we presented an original algorithm, the Weighted K-Order Propagation Number (WKPN) algorithm, to extract the important brain regions associated with WM processes. The simulation revealed that the frontal and posterior regions were activated in two WM states, i.e., update and readout states. Throughout the readout, brain networks performed better in efficiency and resistance to interference. Furthermore, the right prefrontal and parietooccipital regions became more prominent in the completion of extra difficult WM tasks. In summary, these EEG-based results can be taken as promising evidence to understand and improve WM.

1. Introduction

Working memory (WM) is defined as a system that temporarily processes and stores information with restricted capacity in the human brain [1]. It plays an important role in human intelligence and complex cognitive activities such as learning, comprehension, and reasoning. Standard WM states include update, maintenance, and readout [2]. As the objects being remembered are constantly varying, WM adapts to these alterations by updating the stored information with new ones. Another important function of WM is to accurately read information from related brain regions for further cognitive tasks. Studies have shown that during these two states of WM (e.g., update and readout), the brain exhibits abnormal patterns in patients with neurological disorders, such as Attention Deficit Hyperactivity Disorder (ADHD) [3] and Posttraumatic Stress Disorder (PTSD) [4]. Therefore, the study of these two states is of great importance.

Due to the noninvasive and high temporal resolution characteristics, electroencephalography (EEG) has become a popular technique used in the study of human cognitive function [5, 6]. A body of evidence indicates that EEG oscillations in the theta and gamma bands are of particular relevance to WM states. For example, Itthipuripat et al. [7] concluded that the theta power of the frontal cortex increases during the updating state. Polanía et al. [8] decoded contents of visual WM information within high-gamma oscillations in the human prefrontal cortex (PFC) during encoding (that is, updating) and maintenance periods. The research of Semprini et al. [9] likewise validated that theta and gamma oscillations of frontal and posterior areas are associated with updating of memory information, the maintenance of WM, and readout. However, there is

no consensus on the specific oscillation mechanisms corresponding to WM states.

There is increasing recognition that human functional states depend not only on the oscillations of the independent cortices but also on the interactions between a large number of neurons or different regions [10]; consequently, scholars have applied network methods to study information exchange and communication of brain regions [11, 12]. By considering the EEG electrodes as nodes and the statistical relationships between them as edges, a complex brain network can be implemented. In particular, statistical relationships can be quantified using functional connectivity metrics such as Mutual Information [13], Pearson's correlation [14], and Phase Locking Value (PLV) [15]. Since PLV can reflect phase synchronization of signals and interactive coupling and control relationships of different brain regions in a superior degree, it is more suitable for studying the EEG data [16]. As a result, in this study, we construct PLV-based brain networks to investigate the underlying mechanism of WM.

After constructing brain networks, researchers have applied graph theory to analyze network features and probe the human cognitive mechanism and pathogenesis of neurological diseases. As representing the global transmission of information and functional separation in networks, the global efficiency and local efficiency of directed functional networks have been analyzed in Alzheimer's disease in alpha and beta bands [17]. Furthermore, it has been demonstrated that the neural network has a small-world topology [18] that supports simultaneous global and local information processing. The small-worldness index has also been calculated to extract topology descriptors of brain networks to understand WM phases [19].

These indicators are effective in assessing overall network topography but are not at local important brain regions where activities are generally associated with cognitive tasks. For example, Haque et al. [20] suggested that the prefrontal region is vital for WM improvement from the perspective of electrical stimulation. However, evidence of concrete locations of important brain regions is still needed. Currently, algorithms for evaluating important regions of networks include, but are not limited to, weighted degree centrality (WDC) algorithm [21] and weighted betweenness centrality (WBC) algorithm [22]. The WDC algorithm only considered the impact of adjacent nodes on the importance of a node, which cannot reflect the global characteristics. The WBC algorithm considered the global properties but ignored the influence of the node number on the transmission efficiency of the network. To further bridge the local and global characteristics, our team proposed the Weighted K-Order Propagation Number (WKPN) algorithm [23], which introduced a scale factor K that manifests the variation of network properties and enables multiscale analysis of structural changes in networks.

In this paper, we investigate the update and readout states under different loads and study the mechanisms with the WKPN algorithm. Different from the old-fashioned experimental paradigm of memorizing Arabic numerals, we first proposed an original WM paradigm combining alphabet letters with a classical n-back experiment [24]. Then, the neural oscillations and activation brain regions in theta and gamma bands were analyzed. To study the interactions among brain regions, we calculated the PLV of electrode pairs to construct brain networks. Their general topology features were examined by computing global efficiency and local efficiency to assess the small-worldness property. Lastly, the WKPN algorithm was applied to extract the node importance features of brain networks to locate specific sites of key brain regions. The findings are taken as a contribution from an EEG perspective to WM investigations in the future.

2. Materials and Methods

The analysis of WM states can be divided into the following six steps: (1) Designing an experiment to obtain EEG data. (2) Preprocessing raw signals to get analyzable data. (3) Determining the investigated frequency band by time-frequency analysis. (4) Constructing brain networks based on PLV in the determined frequency band. (5) Calculating the properties (e.g., global efficiency and local efficiency) of brain networks. (6) To find the key nodes affecting network properties, the WKPN algorithm is used to locate important brain regions.

2.1. Paradigm. For the purpose of inducing WM with diverse levels of difficulty and load, we devised two n-back experiments with a letter-sequence version (in Figure 1). The lengths of the letter sequence for them were 2 (low WM load) and 4 (high WM load), respectively, and each included 1-back, 2-back, and 3-back tasks. The letters presented were randomly selected from the English alphabet. The presentation of the paradigm was implemented by E-Prime v2.0 (Psychology Software Tools) in this study.

The paradigm started with a cue sign (a black cross) presented in 2 seconds. Subsequently, three groups of letter sequences were displayed in the center of the screen. Subjects are asked to memorize them in order. The duration of every two letters was 3 seconds, and for better memorization, every four letters were presented for 5 seconds. The update state was defined as shown in Figure 1(a). This was followed by a blank picture that lasted 0.5 seconds, which corresponds to the maintenance state. A task cue (a number) of n-back remained on the screen to remind the subjects to recall and record the letter sequence, and this period was considered the readout state. All subjects were required to complete the experiment for the 2 letters condition, then take a 10-minute break to finish the 4 letters condition (in Figure 1(b)). Furthermore, subjects were asked to respond as accurately and quickly as possible, and their reaction time and accuracy were recorded to analyze behavioral performance. Before the formal experiment, a practicing session was prepared for subjects to ensure they were familiar with the entire procedure.

2.2. EEG Recording. The EEG data were recorded with a 500 Hz sampling rate using the NEUROSCAN electrode

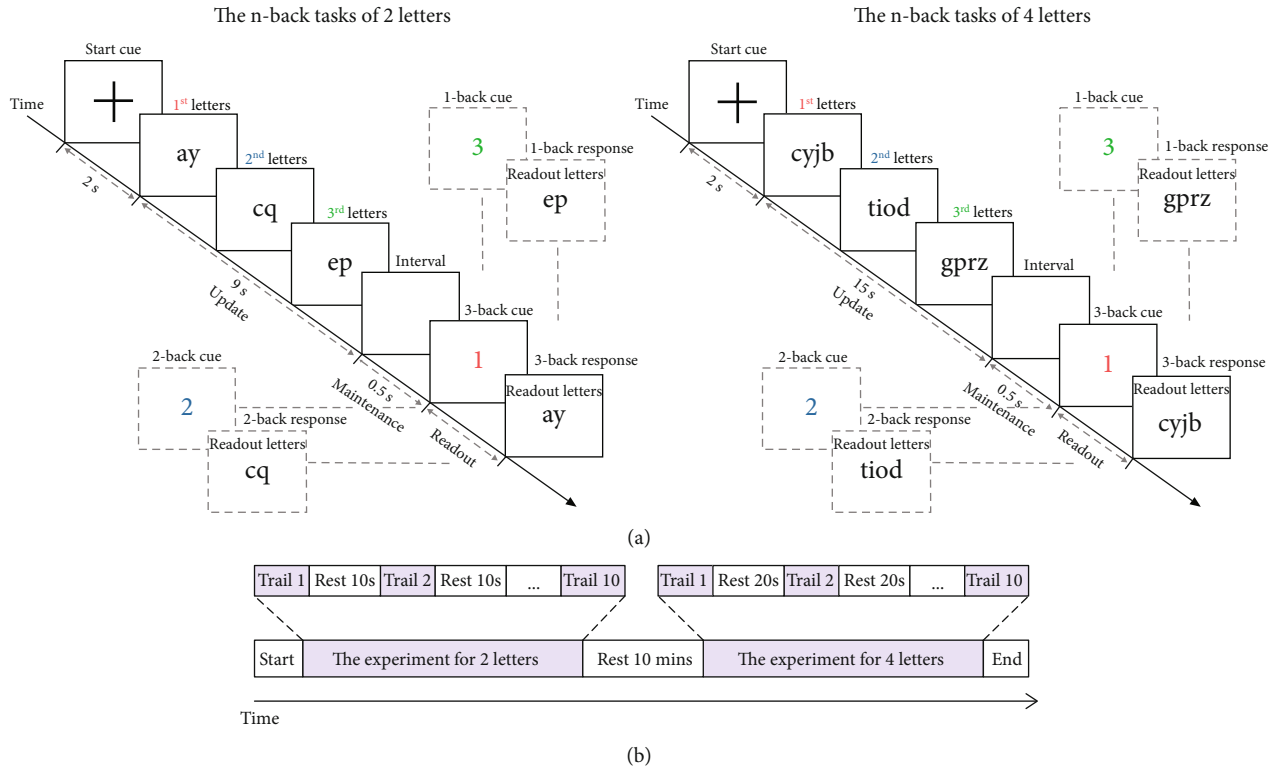

Figure 1: Experimental paradigms and procedure. (a) Paradigms for the n-back ($n = 1, 2, 3$) tasks of 2 letters and 4 letters conditions. (b) The whole experimental procedure.

cap, the SynAmps amplifier, and Curry 7.0 software. The 64 Ag/AgCl electrodes were placed in accordance with the international 10-20 system [25], and the ground electrode was placed on the FZ electrode. The reference electrodes, M1 and M2, were located in the Bilateral mastoid for measurement of myoelectricity, and the additional electrodes HEO and VEO at the outer left and right canthus and up and down the left eye, respectively, for the recording of the movement of the eye. The impedances were kept below 10 kiloohms.

Sixteen healthy students (2 female, age: $M = 23.6$ years old, $SD = 1.2$) were recruited for the experiments, and their participation was rewarded for the better experimental performance. These subjects were right-handed and had no personal or family history of neurological disease. Their memory abilities were all at the same normal level. Before the formal experiment, subjects were prohibited from consuming alcohol and were required to remain sober. Written and oral forms of informed consent were provided, and all subjects chose the latter for convenience. Only subjects who gave their consent were allowed to perform the experiment.

2.3. Data Preprocessing Analysis. Data preprocessing analysis was performed using Brainstorm [26]. The continuous raw data were first filtered with a 0.5-60 Hz bandpass filter to exclude the extra low- and high-frequency component, and with a 50 Hz notch filter to eliminate the power-line interference. The signal artifacts were removed in two steps: first, we manually deleted a small number of signal fragments with significant multiple-channel noise. Then, independent component analysis (ICA) [27] was applied to decompose the EEG data into twenty components. Components of the artifact related to eye movements, muscle activities, and heartbeats were removed. Finally, the artifact-free data were segmented into the update epoch and the readout epoch according to Figure 1. Prior to analysis, the epoch data were removed linear trend and completed baseline correction, where the baseline was the signal from -2 to -0.002 sec for update epoch analysis. For readout epoch analysis, the baseline depended on the length of readout epoch. Readout epochs with incorrect responses were excluded.

2.4. Time-Frequency Analysis. To analyze the time-frequency representation of epoch EEG data in theta and gamma bands, the complex Morlet wavelet transform was performed. The continuous-time signal $x(t)$ was convolved with the complex Morlet wavelet function, $w(t, f)$, to acquire the power spectrum:

$$TF(t, f) = |w(t, f) * x(t)|^2, \quad (1)$$

where t is time and f is frequency. $w(t, f)$ has the shape of a sinusoid, weighted by a Gaussian kernel [28], and it can be expressed as

$$w(t, f) = Ae^{\left(-t^2/2\sigma_t^2\right)} e^{i2\pi ft}, \quad (2)$$

where σ_t is the standard variation of the Morlet wavelet in the time domain, $A = (\sigma_t\sqrt{\pi})^{-1/2}$, $i = \sqrt{-1}$. The resolution

of complex Morlet wavelet transform is given in units of Full-Width Half Maximum of the Gaussian kernel, both in time and frequency. The frequencies were reorganized into two frequency bands (theta (4-8 Hz) and gamma (30-60 Hz)) closely related to the WM process.

We divided epoch data into several trials and averaged the time-frequency spectra of the subject across all trials to conclude which brain regions were activated at specific frequency bands. Statistics on power changes were performed by one-way ANOVA (significant level is 5%). The significant frequency bands in WM states were analyzed and chosen for the follow-up brain network construction.

2.5. Complex Brain Network Analysis

2.5.1. Constructing Brain Network. The human brain can be seen as a complex network formed with specific connectivity patterns [29]. We created PLV brain networks in theta and gamma bands. At first, information in the two bands of epochs data (baseline excluded) was extracted, and then the Hilbert Transform [30] was performed on a pair of electrode signals $x(t)$ and $y(t)$ to obtain their analytic signals $z_x(t)$ and $z_y(t)$, according to the equations (3) and (4),

$$z_x(t) = x(t) + iHT(x(t)), \tag{3}$$

$$z_y(t) = y(t) + iHT(y(t)). \tag{4}$$

The relative phase $\Delta\phi(t)$ between $z_x(t)$ and $z_y(t)$ was also computed, and the corresponding PLV [31] was calculated as,

$$PLV_{xy} = \left| \frac{1}{n} \sum_{k=1}^{n} e^{i\Delta\phi(t_k)} \right|, \tag{5}$$

where n is the total number of data points and t_k is a data point. Note that according to its definition, PLV always takes values between 0 and 1. The larger the PLV, the stronger the phase synchronization of the two signals, and 1 signifies that one signal completely follows the other. Finally, the electrodes were considered nodes, and the PLV values were viewed as the weights of edges to construct the weighted brain networks with 62 nodes (the M1 and M2 electrodes were excluded).

2.5.2. Global Efficiency and Local Efficiency. Global efficiency reflects the efficiency of information exchange of a network, and local efficiency corresponds to network robustness. According to the literature [32], small-world networks have both high global efficiency and local efficiency. Therefore, after constructing the PLV networks, we selected the two indices to evaluate the small-worldness to describe the general topological properties of the networks. Global efficiency and local efficiency were calculated using the Brain Connectivity Toolbox developed for the MATLAB environment.

Since the efficiency of the communication between nodes v_i and v_j can be expressed as the inverse of the shortest path, $1/d_{ij}$, between them, the global efficiency of the brain network is defined as the average of the inverse of the shortest paths among all node pairs [33],

$$E_{\text{global}} = \frac{1}{n(n-1)} \sum_{i \neq j} \frac{1}{d_{ij}}, \tag{6}$$

where $n = 62$. Note that if v_i is not connected to v_j, then d_{ij} is equal to ∞. The value of E_{global} ranges from 0 to 1, and the larger the value, the better the ability to exchange information within the network.

Rows and columns corresponding to node v_i ($i = 1, 2, \cdots, n$) in adjacency matrix A were deleted, and then n subnetworks S_i were constructed. Local efficiency of the network is introduced as the average global efficiency of all subnetworks [34],

$$E_{\text{local}} = \frac{1}{n} \sum_{i=1}^{N} E_{\text{global}}(S_i). \tag{7}$$

The local efficiency assesses the ability of information transmission of the network in the absence of a certain node.

Any changes in global and local efficiency related to the different conditions (update, readout, 2 letters, 4 letters, n-back tasks) were evaluated by means of statistical comparison, a one-way ANOVA method. This test was taken for all subjects and the significance level was set at 5%.

2.5.3. Weighted K-Order Propagation Number Algorithm. Considering that the WKPN algorithm was proposed based on the comprehensive examination of the local and global properties of networks, we used it to assess the specific locations of important brain regions.

The WKPN algorithm abstracts the disease transmission based on the network topology. Each node was set as the source of infection separately, and after a certain propagation time, the node importance was obtained based on the number of infected nodes in the network. When the value of propagation time is small, the result reflects the local characteristic of the network, and as the time value increases, it corresponds to the global property. Simulations showed that this method can thoroughly portray the impact of long-distance connections on information transmission in small-world networks and can also increase the importance of bridge nodes [35].

The steps of the WKPN algorithm are explained in detail as follows. Based on the adjacency matrix A (62×62) of the network, the shortest paths of all node pairs were calculated. The propagation time K is defined as the values of the shortest paths, namely, $K \in [0, d]$, and d is the diameter of the weighted network. The number of nodes that a node v_i can reach within K is considered the K-order propagation number $N_{v_i}^K$, and it was combined with the information entropy to calculate the K-order structural entropy of the brain network,

$$H^K = -\sum_{i=1}^{n} \frac{N_{v_i}^K}{\sum_{j=1}^{n} N_{v_j}^K} \log \left(\frac{N_{v_i}^K}{\sum_{j=1}^{n} N_{v_j}^K} \right), \tag{8}$$

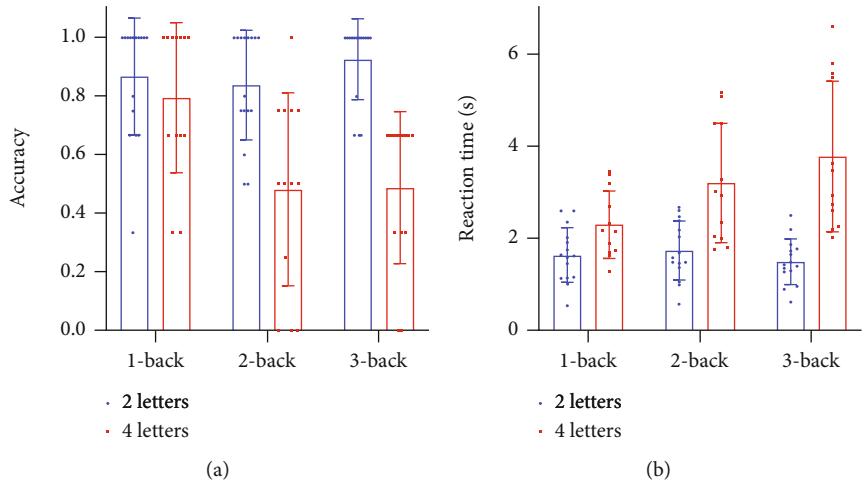

FIGURE 2: Behavioral performance of all subjects. (a) Response accuracy. (b) Reaction time. Statistics were performed using the paired sample t test with a 95% confidence interval. A single data point represents a subject. Error bars represent standard deviation (SD).

where n is the number of nodes, equal to 62 based on previous work. Subsequently, the node importance of v_i is defined by considering the comprehensive evaluation from $K = 0$ to $K = d$, according to the formula,

$$Q_{v_i} = \sum_{K=0}^{d} \left(1 - \frac{H^K - \min(H)}{\max(H) - \min(H)}\right) \left(\frac{N_{v_i}^K - \min\left(N^K\right)}{\max\left(N^K\right) - \min\left(N^K\right)}\right), \tag{9}$$

where $H = \{H^0, H^1, \cdots, H^d\}$ and $N^K = \{N_{v_1}^K, N_{v_2}^K, \cdots, N_{v_n}^K\}$. Eventually, the nodes of the PLV networks were ranked from highest to lowest importance to obtain vital brain regions. The algorithm has been validated to be effective for the assessment of important nodes in complex networks [35].

3. Results and Discussion

3.1. Behavioral Results. We recorded and analyzed the behavioral performance of all subjects during the experiments. As shown in Figure 2, response accuracy usually decreased and reaction time increased as the difficulty of the n-back task and WM load increased. However, interestingly, in the 3-back task, the accuracy was higher ($p = 0.085$) and the reaction time was shorter ($p < 0.05$) as compared to the 2-back task in the 2 letters condition. This is contrary to the perception that the harder the task, the lower the response accuracy. We speculated that the memory target of the 3-back is the initial appearance which has an impressive effect on the brain to elicit better WM behavioral results under the low load condition.

3.2. Results of EEG Power. The topographical maps of time-averaged power in theta and gamma bands are reported in Figure 3. For the low WM load condition (in Figure 3(a)), the midfrontal and posterior regions were activated at the theta band in both update and readout states. Theta power was generally higher in the update state than in readout ($p < 0.05$, $p < 0.05$), which is consistent with the fact that theta oscillations in these two regions have a vital impact on WM update[36]. During update and readout, the gamma power was increased in the occipital lobe, possibly indicating that the posterior region plays an important role in integrating and processing visual stimuli in our experiment.

Under the high WM load condition (in Figure 3(b)), the frontal and posterior regions were activated more strongly in theta band compared to under the low load condition during the update ($p < 0.05$, $p < 0.05$). It means that the oscillations were strengthened with WM load increasing. However, we did not find a clear pattern in the power changes of the activated regions during readout. Considering that the response accuracy in the 2-back and 3-back tasks had been as low as 50%, we believed that 12 letters may have exceeded the WM capacities of subjects, and thus for them, there was no difference among the n-back tasks.

The differences of theta power in readout state under low WM load were calculated at a representative electrode (FZ) of the midfrontal region where the power peaked in the n -back tasks (in Figure 4). The theta power of the FZ electrode in the 3-back task was lower than that in the 2-back task ($p < 0.05$), which is contrary to the conclusion related to the difficulty factor of the tasks. This trend echoes the behavioral results, and our conjecture that the memory content with first presence makes a strong impression has been verified.

3.3. Topological Properties of PLV Brain Networks. The global efficiency and the local efficiency of all brain networks are demonstrated in Figure 5. As shown in the box plots, the global efficiency and local efficiency were generally higher in readout as compared to those in the update state. It indicates that brain networks have higher small-world properties; namely, they are more capable of transmitting information globally and more resistant to interference. Furthermore, we found that global efficiency and local efficiency in readout were higher under low load condition. Given the lower response accuracy in behavioral results, we suggest that the

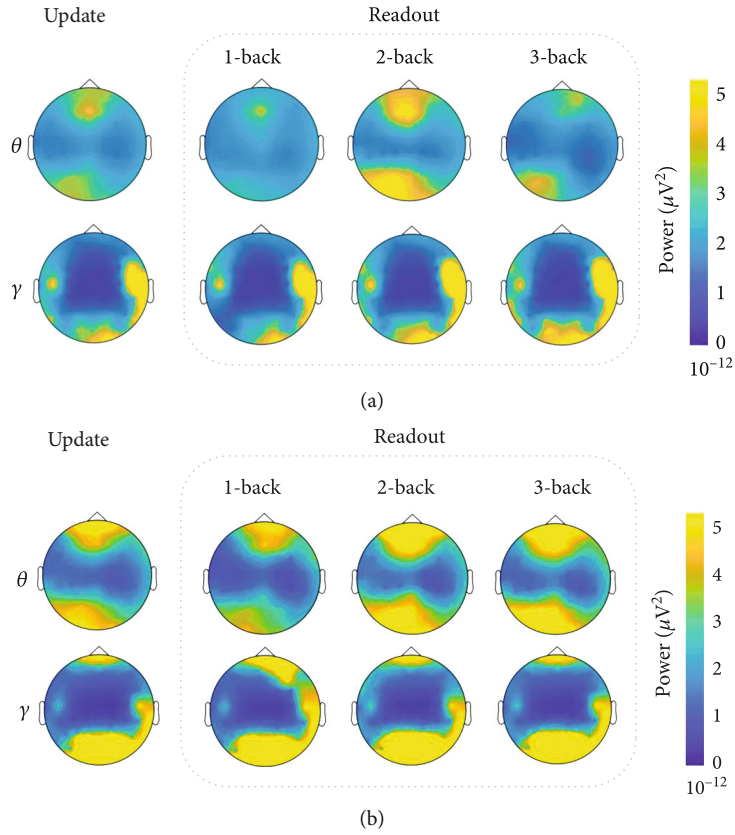

FIGURE 3: Topographic maps of the theta and gamma power in update and readout states for an example subject. (a) 2 letters condition. (b) 4 letters condition.

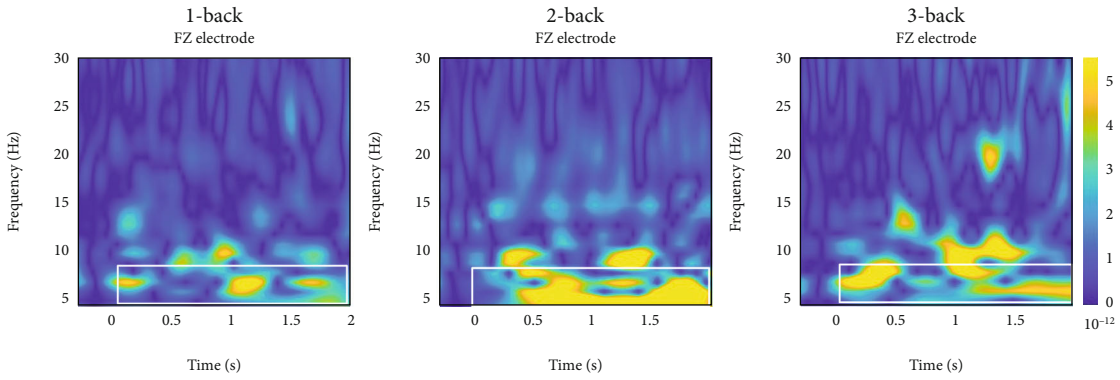

FIGURE 4: Time-frequency power plots (after baseline correction) from a representative midfrontal electrode (FZ) for 1-back, 2-back, and 3-back tasks for an example subject. The area marked in white is the theta band.

small-worldness of the brain is reduced under high WM load condition, especially when it exceeds the individual's capacity.

We ranked the importance of all nodes in order from the highest to the lowest based on the WKPN algorithm. The top five important nodes of the PLV networks and their first five edges with the highest weights are shown in Figure 6. Figure 6(a) illustrates that important brain regions in both update and readout states are concentrated in the frontal and parietooccipital lobes for low WM load condition. It is consistent with the results of time-frequency analysis and reflects the processing of visual information in the occipital lobe [37] and the executive control of the frontal region [38] during the WM task in terms of synchrony. In the theta band, the frontal regions were more tightly connected in readout. With the increase of difficulties of n-back tasks, the node importance of the right prefrontal electrodes became greater, especially the AF4 electrode, and the number of important nodes in the parietooccipital region was growing. It indicates that the interactive coupling and control relationships in the two regions intensified with the increase of task complexity. In particular, it has been

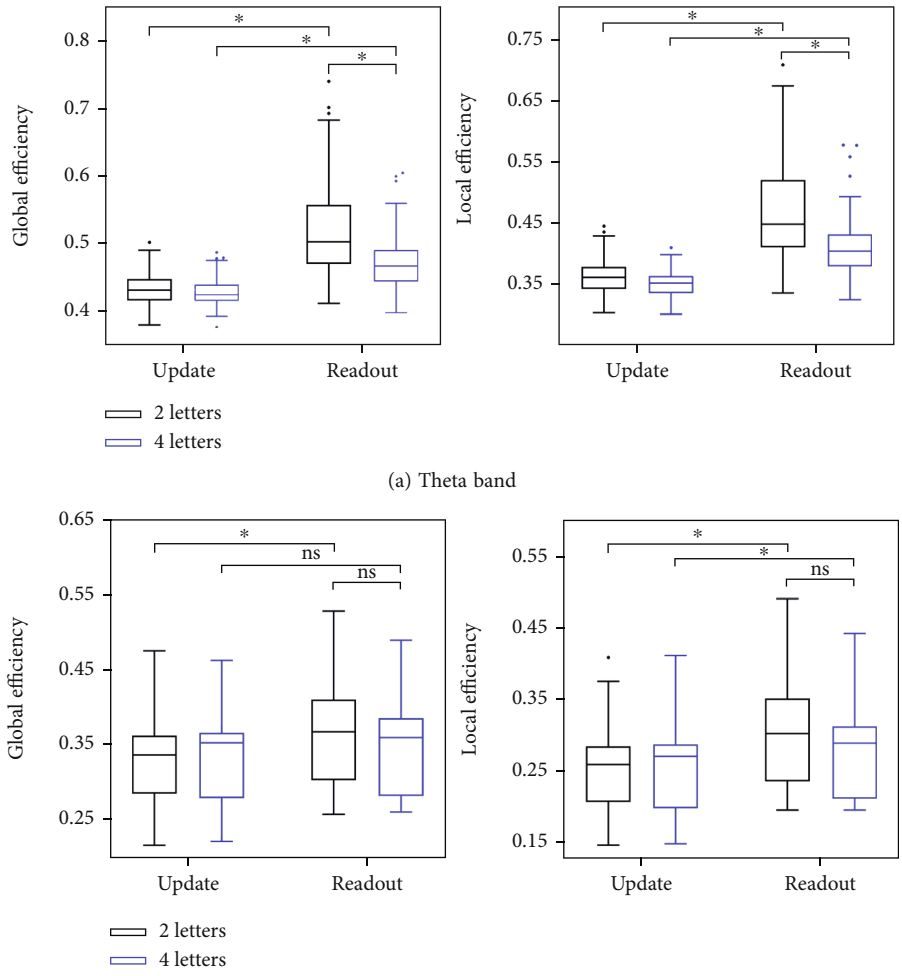

(a) Theta band

(b) Gamma band

Figure 5: The box plots for 2 and 4 letters conditions. Global efficiency and local efficiency of all brain networks relative to the update and readout states were computed at (a) the theta band and (b) the gamma band. A single data point represents a brain network. The asterisks indicate $p < 0.05$ and the ns means $p > 0.05$.

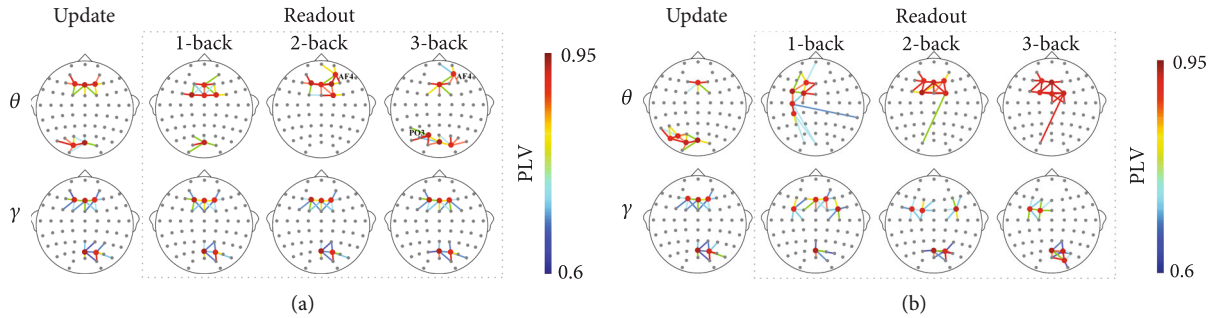

(a) (b)

Figure 6: The top five important nodes and their first five edges in theta and gamma bands were chosen to represent the significant brain regions and the connections in update and readout states for (a) 2 letters condition and (b) 4 letters condition. In the readout of the 4 letters condition, only the brain network map of an example subject is shown because of the large inter-subject variation in reading effects. The others are maps of the brain network averaged across subjects.

proposed that the left hemisphere is relative to verbal information and logical reasoning, while the right is responsible for spatial thinking [39]. Therefore, it can be assumed that as the difficulties of WM tasks increase, the brain may convert verbal information into spatial information to better extract memory content. In the gamma band, there was no

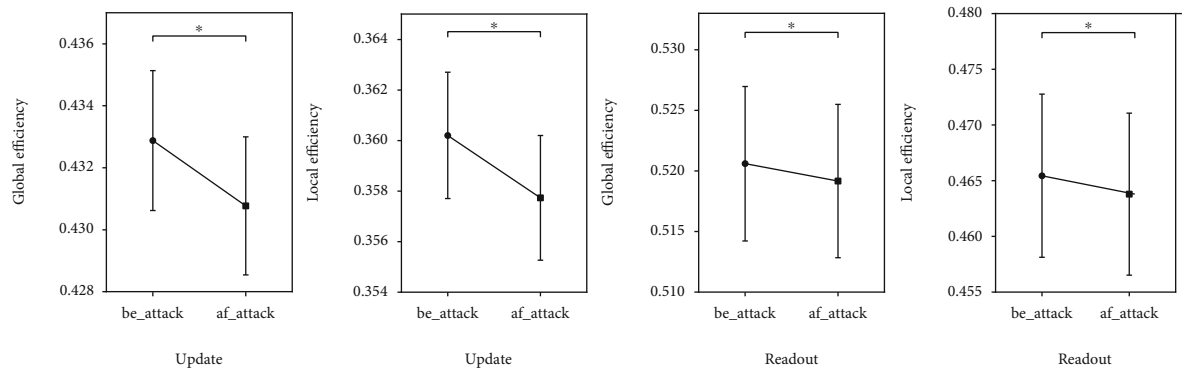

Figure 7: Global efficiency and local efficiency in theta band for the 2 letters condition before and after attacks on the networks. The be_attack represents before the attack and the af_attack after. Error bars represent the standard error of mean (SEM) of properties in brain networks for all subjects. The asterisks indicate $p < 0.05$.

significant difference between the important brain regions which were mainly located in the frontal and right parietooccipital regions in the two states.

For the high load condition, the parietooccipital region became more vital in update in the theta band (Figure 6(b)), which is perhaps related to the increased visual information in our paradigm. However, in readout state, there was no clear trend in the distribution and connection of important brain regions. This further validates the tasks in 4 letters condition are so challenging that there is no difference between the *n*-back tasks for subjects.

Based on the above findings, we attacked the important node (FZ) of brain networks in update and AF4 in readout, as well as calculated global efficiency and local efficiency again. As shown in Figure 7, these two indexes dropped significantly after the networks were attacked. This implies that these key nodes play a significant role in strengthening the efficiency of information transfer of the brain network. Thus, the stronger small-worldness of brain networks in readout might be related to the enhanced importance of the right-hand nodes.

4. Conclusions

In this paper, EEG data collected with a novel letter-sequence version of *n*-back pattern were used to research WM update and readout states. Time-frequency analysis was applied to investigate activated brain regions and the conversion of their power. The PLVs of electrode pairs were calculated to construct complex brain networks, and then the topological characteristics of the PLV networks were considered by calculating global and local efficiency to assess the small-worldness. Ultimately, the WKPN algorithm was leveraged to divulge the specific location of crucial brain regions from the perspective of the synchronization and control relationships.

Based on the aforementioned approaches, the principal conclusions can be summarized as follows: (1) In terms of both power and synchrony, the frontal and parietooccipital regions each have an important impact on the WM update and readout states. (2) The brain networks have higher global and local efficiency during WM readout. (3) The importance of the right prefrontal region (such as AF4) and the parietooccipital region (such as PO3) increases in the readout state under more difficult WM tasks. (4) The first memory target achieves higher accuracy in a lower load condition.

The WKPN algorithm is verified to be effective by locating and attacking network critical nodes. This means that we provide a new way from a brain network perspective to track important regions at the sensor level. It is helpful for some intensive research, such as transcranial electrical stimulation (tES) [40]. Selection of stimulus points is based on the locations obtained from the algorithm rather than a priori knowledge, which can improve the effectiveness of stimuli. Moreover, considering that the EEG technique acquires scalp signals, source localization [41] is expected to be applied to survey the deeper level of brain mechanisms in future work.

Data Availability

Raw data are available via a request to the lead author with the need of a formal data-sharing agreement.

Conflicts of Interest

The authors declare that the research was conducted in the absence of commercial or financial relationships that could be construed as a potential conflict of interest.

Acknowledgments

This study was funded by the National Natural Science Foundation of China (grant number 61977039) and the 2019 Research Project of University Education Informatization (grant number 2019JSETKT009).

References

[1] A. Baddeley, "Working memory: looking back and looking forward," *Nature Reviews Neuroscience*, vol. 4, no. 10, pp. 829–839, 2003.

[2] B. Rypma and M. D'Esposito, "Isolating the neural mechanisms of age-related changes in human working memory," *Nature Neuroscience*, vol. 3, no. 5, pp. 509–515, 2000.

[3] H. A. D. Keage, C. R. Clark, D. F. Hermens et al., "ERP indices of working memory updating in AD/HD: differential aspects of development, subtype, and medication," *Journal of Clinical Neurophysiology*, vol. 25, no. 1, pp. 32–41, 2008.

[4] C. Galletly, C. R. Clark, A. C. McFarlane, and D. L. Weber, "Working memory in posttraumatic stress disorder—an event-related potential study," *Journal of Traumatic Stress*, vol. 14, no. 2, pp. 295–309, 2001.

[5] S. Ahrens, J. D. Twanow, J. Vidaurre, S. Gedela, M. Moore-Clingenpeel, and A. P. Ostendorf, "Electroencephalography technologist inter-rater agreement and interpretation of pediatric critical care electroencephalography," *Pediatric Neurology*, vol. 115, pp. 66–71, 2021.

[6] S. Singla, G. E. Garcia, G. E. Rovenolt et al., "Detecting seizures and epileptiform abnormalities in acute brain injury," *Current Neurology and Neuroscience Reports*, vol. 20, no. 9, p. 42, 2020.

[7] S. Itthipuripat, J. R. Wessel, and A. R. Aron, "Frontal theta is a signature of successful working memory manipulation," *Experimental Brain Research*, vol. 224, no. 2, pp. 255–262, 2013.

[8] R. Polanía, W. Paulus, and M. A. Nitsche, "Noninvasively decoding the contents of visual working memory in the human prefrontal cortex within high-gamma oscillatory patterns," *Journal of Cognitive Neuroscience*, vol. 24, no. 2, pp. 304–314, 2012.

[9] M. Semprini, G. Bonassi, F. Barban et al., "Modulation of neural oscillations during working memory update, maintenance, and readout: an hdEEG study," *Human Brain Mapping*, vol. 42, no. 4, pp. 1153–1166, 2021.

[10] C. W. Lynn and D. S. Bassett, "The physics of brain network structure, function and control," *Nature Reviews Physics*, vol. 1, no. 5, pp. 318–332, 2019.

[11] A. P. Alivisatos, A. M. Andrews, E. S. Boyden et al., "Nanotools for neuroscience and brain activity mapping," *ACS Nano*, vol. 7, no. 3, pp. 1850–1866, 2013.

[12] J. M. Bernabei, T. C. Arnold, P. Shah et al., "Electrocorticography and stereo EEG provide distinct measures of brain connectivity: implications for network models," *Brain Communications*, vol. 3, no. 3, 2021.

[13] R. A. Thuraisingham, "Estimating electroencephalograph network parameters using mutual information," *Brain Connectivity*, vol. 8, no. 5, pp. 311–317, 2018.

[14] J. Gao, W. Wang, and J. Zhang, "Explore interregional EEG correlations changed by sport training using feature selection," *Computational Intelligence and Neuroscience*, vol. 2016, Article ID 6184823, 2016.

[15] A. M. Gong, J. P. Liu, L. Lua, G. R. Wu, C. H. Jiang, and Y. F. Fu, "Characteristic differences between the brain networks of high-level shooting athletes and non-athletes calculated using the phase-locking value algorithm," *Biomedical Signal Processing and Control*, vol. 51, pp. 128–137, 2019.

[16] Z. M. Wang, Y. Tong, and X. Heng, "Phase-locking value based graph convolutional neural networks for emotion recognition," *IEEE Access*, vol. 7, pp. 93711–93722, 2019.

[17] S. Afshari and M. Jalili, "Directed functional networks in Alzheimer's disease: disruption of global and local connectivity measures," *IEEE Journal of Biomedical and Health Informatics*, vol. 21, no. 4, pp. 949–955, 2017.

[18] N. Franzmeier, J. Hartmann, A. N. W. Taylor et al., "The left frontal cortex supports reserve in aging by enhancing functional network efficiency," *Alzheimer's Research & Therapy*, vol. 10, no. 1, p. 28, 2018.

[19] J. Toppi, L. Astolfi, M. Risetti et al., "Different topological properties of EEG-derived networks describe working memory phases as revealed by graph theoretical analysis," *Frontiers in Human Neuroscience*, vol. 11, p. 637, 2017.

[20] Z. Z. Haque, R. Samandra, and F. A. Mansouri, "Neural substrate and underlying mechanisms of working memory: insights from brain stimulation studies," *Journal of Neurophysiology*, vol. 125, no. 6, pp. 2038–2053, 2021.

[21] T. Opsahl, F. Agneessens, and J. Skvoretz, "Node centrality in weighted networks: generalizing degree and shortest paths," *Social Networks*, vol. 32, no. 3, pp. 245–251, 2010.

[22] H. J. Wang, J. M. Hernandez, and P. Van Mieghem, "Betweenness centrality in a weighted network," *Physical Review. E, Statistical, Nonlinear, and Soft Matter Physics*, vol. 77, no. 4, article 046105, 2008.

[23] P. C. Tang, C. C. Song, W. W. Ding, J. K. Ma, J. Dong, and L. Y. Huang, "Research on the node importance of a weighted network based on the K-order propagation number algorithm," *Entropy*, vol. 22, no. 3, p. 364, 2020.

[24] W. K. Kirchner, "Age differences in short-term retention of rapidly changing information," *Journal of Experimental Psychology*, vol. 55, no. 4, pp. 352–358, 1958.

[25] H. Jasper, "The ten-twenty electrode system of the international federation," *Electroencephalography and Clinical Neurophysiology*, vol. 10, pp. 371–375, 1958.

[26] F. Tadel, S. Baillet, J. C. Mosher, D. Pantazis, and R. M. Leahy, "Brainstorm: a user-friendly application for MEG/EEG analysis," *Computational Intelligence and Neuroscience*, vol. 2011, Article ID 879716, 2011.

[27] C. Jutten and J. Herault, "Blind separation of sources, part I: an adaptive algorithm based on neuromimetic architecture," *Signal Processing*, vol. 24, no. 1, pp. 1–10, 1991.

[28] J. Yordanova, V. Kolev, and A. Rothenberger, "Event-related oscillations reflect functional asymmetry in children with attention deficit/hyperactivity disorder," *Supplements to Clinical Neurophysiology*, vol. 62, pp. 289–301, 2013.

[29] A. M. Bastos and J.-M. Schoffelen, "A tutorial review of functional connectivity analysis methods and their interpretational pitfalls," *Frontiers in Systems Neuroscience*, vol. 9, p. 175, 2015.

[30] M. Le Van Quyen, J. Foucher, J.-P. Lachaux et al., "Comparison of Hilbert transform and wavelet methods for the analysis of neuronal synchrony," *Journal of Neuroscience Methods*, vol. 111, no. 2, pp. 83–98, 2001.

[31] J. P. Lachaux, E. Rodriguez, J. Martinerie, and F. J. Varela, "Measuring phase synchrony in brain signals," *Human Brain Mapping*, vol. 8, no. 4, pp. 194–208, 1999.

[32] V. Latora and M. Marchiori, "Efficient behavior of small-world networks," *Physical Review Letters*, vol. 87, no. 19, article 198701, 2001.

[33] T. P. Zhang, B. Fang, and X. Y. Liang, "A novel measure to identify influential nodes in complex networks based on network global efficiency," *Modern Physics Letters B*, vol. 29, no. 28, pp. 1550168–1550442, 2015.

[34] M. L. Stanley, S. L. Simpson, D. Dagenbach, R. G. Lyday, J. H. Burdette, and P. J. Laurienti, "Changes in brain network efficiency and working memory performance in aging," *PLoS One*, vol. 10, no. 4, article e0123950, 2015.

[35] Y. H. Zhang, Y. Liao, Y. D. Zhang, and L. Y. Huang, "Emergency braking intention detect system based on K-order propagation number algorithm: a network perspective," *Brain Sciences*, vol. 11, no. 11, p. 1424, 2021.

[36] R. J. Zhu, Y. M. Luo, Z. Y. Wang, and X. Q. You, "Modality effects in verbal working memory updating: transcranial direct current stimulation over human inferior frontal gyrus and posterior parietal cortex," *Brain and Cognition*, vol. 145, p. 8, 2020.

[37] A. Sugiura, B. H. Silverstein, J.-W. Jeong et al., "Four-dimensional map of direct effective connectivity from posterior visual areas," *NeuroImage*, vol. 210, article 116548, 2020.

[38] B. Griesmayr, B. Berger, R. Stelzig-Schoeler, W. Aichhorn, J. Bergmann, and P. Sauseng, "EEG theta phase coupling during executive control of visual working memory investigated in individuals with schizophrenia and in healthy controls," *Cognitive, Affective, & Behavioral Neuroscience*, vol. 14, no. 4, pp. 1340–1355, 2014.

[39] Z. T. Ren, Y. Zhang, H. He, Q. Y. Feng, T. Y. Bi, and J. Qiu, "The different brain mechanisms of object and spatial working memory: voxel-based morphometry and resting-state functional connectivity," *Frontiers in Human Neuroscience*, vol. 13, p. 248, 2019.

[40] K. Ergo, E. De Loof, G. Debra, B. Pastotter, and T. Verguts, "Failure to modulate reward prediction errors in declarative learning with theta (6 Hz) frequency transcranial alternating current stimulation," *PLoS One*, vol. 15, no. 12, article e0237829, 2020.

[41] J. M. Schoffelen and J. Gross, "Source connectivity analysis with MEG and EEG," *Human Brain Mapping*, vol. 30, no. 6, pp. 1857–1865, 2009.